Identification of P218 as a potent inhibitor of *Mycobacteria ulcerans* DHFR

Gustavo Pelicioli Riboldi,[ab] Rachael Zigweid,[c] Peter J. Myler,[cd] Stephen J. Mayclin,[ef] Rafael Miguez Couñago,[ab]* Bart L. Staker*[c]

[a.] *Centro de Química Medicinal (CQMED), Centro de Biologia Molecular e Engenharia Genética (CBMEG), Universidade Estadual de Campinas (UNICAMP), Campinas, SP, 13083-875, Brazil.*

[b.] *Structural Genomics Consortium, Departamento de Genética e Evolução, Instituto de Biologia, UNICAMP, Campinas, SP, 13083-886, Brazil.*

[c.] *Center for Infectious Disease Research, Seattle Children's Research Institute, Seattle, Washington, 98109, USA.*

[d.] *Department of Pediatrics, University of Washington, Seattle, Washington, 91895, USA.*

[e.] *Seattle Structural Genomics Center for Infectious Disease (SSGCID), Seattle, Washington 98109, USA*

[f.] *UCB, Bainbridge Island, Washington 98110, USA*

* rafael.counago@unicamp.br; bart.staker@seattlechildrens.org

Abstract (50-250 words)

Mycobacterium ulcerans is the causative agent of Buruli ulcer, a debilitating chronic disease that mainly affects the skin. Current treatments for Buruli ulcer are efficacious, but rely on the use of antibiotics with severe side effects. The enzyme dihydrofolate reductase (DHFR) plays a critical role in the de novo biosynthesis of folate species and is a validated target for several antimicrobials. Here we describe the biochemical and structural characterization of *M. ulcerans* DHFR and identified P218, a safe antifolate compound in clinical evaluation for malaria, as a potent inhibitor of this enzyme. We expect our results to advance *M. ulcerans* DHFR as a target for future structure-based drug discovery campaigns.

Introduction

Buruli ulcer is a necrotizing skin disease caused by *Mycobacterium ulcerans* infection. Skin ulcers are a result of the host immune response to mycolactone, an immunosuppressive polyketide-derived macrolide cytotoxin secreted by *M. ulcerans*[1–3]. Buruli ulcer is considered a major public health problem in endemic areas[4], which include humid rural tropical zones prone to seasonal flooding and/or linked to low-lying wetland areas[5,6]. Current treatment - oral (rifampin) and injectable (streptomycin) antibiotics - is effective but requires daily antibiotic injections for 8 weeks and is associated with long-term hearing loss[7]. Thus, a major goal of Buruli ulcer research is finding an all-oral therapeutic strategy that shortens the duration of treatment and avoids severe side-effects[8,9].

Unlike mammals, microbes are unable to obtain folate from the environment and rely on *de novo* production of reduced folate species for the biosynthesis of critical cellular components, including methionine, glycine, serine, *N*-formylmethionyl-tRNA, purines, and thymidine[10,11]. Thus, folate metabolism is a vulnerable pathway in microbes and antifolate compounds have found widespread use in the clinic. Two enzymes in the microbial folate pathway are validated targets for antifolate compounds: dihydropteroate synthase (DHPS), and dihydrofolate reductase (DHFR). Compounds inhibiting these enzymes are effective against pathogenic *Mycobacterium* species, including *M. ulcerans*[12,13], *M. leprae*[14–17], the causative agent of leprosy, and *M. tuberculosis*[11,18–20], the causative agent of tuberculosis. In the clinic, dapsone, (DDS; diaminodiphenyl sulfone) a sulfone antibiotic targeting DHPS, is used with rifampicin and clofazimine to treat leprosy and *p*-aminosalicylic acid (PAS), a prodrug targeting DHFR[21], is a second-line treatment for tuberculosis. Nevertheless, the treatment of Buruli ulcer or other mycobacterial infections with antifolates remains incompletely explored.

As in other mycobacteria, *M. ulcerans* (Mul)DHFR is encoded by a single gene (*dfrA* or *folA*)[22]. The MulDHFR amino acid sequence is 74, 28, and 32% identical to *M. tuberculosis* (Mtb), *Staphylococcus aureus* (Sau) and *Escherichia coli* (Eco)DHFR, respectively. While trimethoprim (TMP), a diaminopyrimidine antibiotic used against both Gram-positive and Gram-negative bacteria, is a potent inhibitor of Eco- and

SauDHFR[23], TMP is ineffective against *M. tuberculosis* and *M. ulcerans*. However, combining dapsone with epiroprim, a different diaminopyrimidine antibiotic that targets DHFR, is effective in culture against *M. ulcerans*[13,15,24].

Despite differences in amino acid sequence, bacterial and human DHFR enzymes have a conserved structural architecture consisting of two distinct sub-domains. The adenosine binding subdomain provides the binding site for the NADPH cofactor adenosine moiety. The major (or "loop") sub-domain encompasses most of the protein and has three loop regions - M20, F-G, and G-H; important for substrate binding and enzyme catalysis[25]. Amino acid differences in the "loop" subdomain are thought to be responsible for determining inhibitor selectivity towards DHFR in different organisms. Mutations to residues in this subdomain are associated with the emergence of bacterial strains resistant to anti-folate antibiotics, mainly in Gram-negative bacteria[26–28].

Focused medicinal chemistry efforts have produced potent and cell-permeable DHFR inhibitors that are efficacious against *M. tuberculosis*[18–20]. To enable similar programs for Buruli ulcer, we report here the biochemical and structural characterization of MulDHFR and the identification of P218 - a DHFR inhibitor undergoing clinical studies as a therapy for malaria - as a potent MulDHFR inhibitor. We expect our work to contribute to the development of future therapeutic strategies for Buruli ulcer based on anti-folates.

Experimental

Gene cloning and Recombinant Protein Production. Cloning, expression and purification were conducted as part of the Seattle Structural Genomics Center for Infectious Disease (SSGCID)[29,30] following standard protocols described previously[31–33]. Prokaryotic expression vectors containing either the wild-type (WT) or the cysteine-89 variant mutant (C89S) of *M. ulcerans* DHFR were obtained from the Seattle Structural Genomics Center for Infectious Disease (clone ID MyulA.01062.a.B1.GE39104 and MyulA.01062.a.B11.GE42658, respectively; www.SSGCID.org). The C89S variant was created by performing Site-Directed Mutagenesis on the WT using a Quick-Change Lightning Kit, based upon the UCLA MBI-SERp Server Identification of high surface-

entropy residues. Primers were designed using the Quick-Change Primer Design Program available online at www.agilent.com/genomics/qcpd.

The gene was cloned into the ligation independent cloning (LIC) expression vector pBG1861 encoding a non-cleavable, N-terminal 6xHis fusion tag (amino acid sequence: MAHHHHHH)[31]. Plasmid DNA was transformed into chemically competent *E. coli* BL21(DE3)R3 Rosetta cells. The plasmids containing MulDHFR and MulDHFR-C89S were expression tested and 2 litres of culture were grown using auto-induction media[34] in a LEX Bioreactor (Epiphyte Three Inc.) as previously described[35].

MulDHFR and MulDHFR-C89S were purified in a two-step protocol consisting of a Ni^{2+}-affinity chromatography (IMAC) step and size-exclusion chromatography (SEC). All chromatography runs were performed on an ÄKTApurifier 10 (GE) using automated IMAC and SEC programs according to previously described procedures[33]. Bacterial pellets -thawed in a 42 °C water bath and vortexed gently were resuspended in 180 ml lysis buffer containing 20 mM HEPES pH 7.2-7.4, 300 mM NaCl, 5% (v/v) glycerol, 0.5% CHAPS, 30 mM Imidazole, 21 mM $MgCl_2$, 1 mM TCEP, and 2 protease inhibitor tablets and lysed by sonication for 15 minutes (5 sec on, 10 sec off, 70% amplitude, on ice). After sonication, the crude lysate was clarified with 2 µl of Benzonase and incubated while mixing at room temperature for 45 minutes. The lysate was then clarified by centrifugation at 10,000 rev min^{-1} for 1h at 4° C using a Sorvall centrifuge (Thermo Scientific). The supernatant was filtered through a 0.45 µM syringe filter, then passed over a Ni-NTA His-Trap FF 5 ml column (GE Healthcare) which was pre-equilibrated with loading buffer composed of 20 mM HEPES pH 7.0, 300 mM NaCl, 5% (v/v) glycerol, and 30 mM Imidazole. The column was washed with 20 column volumes (CV) of loading buffer and was eluted with 10 CVs of loading buffer plus 0.5 M imidazole. Peak fractions, as determined by UV at 280 nm, were pooled and concentrated to 5 ml with a 3K Pall filter. A SEC column (Superdex 75, GE) was equilibrated with running buffer composed of 300 mM NaCl, 20 mM HEPES pH 7.0, 5% (v/v) glycerol, and 1 mM TCEP. The peak fractions were collected and analysed for the presence of the protein of interest using SDS–PAGE. The peak fractions were pooled and concentrated using an Amicon purification system (Millipore). Aliquots of 110 µl were flash-frozen in a dry ice and ethanol bath and stored at −80°C until use. The protein was quantitated by UV-light (extinction coefficient of 37,470 M^{-1} cm^{-1}) using a Nanodrop spectrophotometer

(Thermo). The molecular mass of the purified protein was confirmed by intact mass, LC-MS.

Enzyme assays. Dihydrofolate reductase enzyme activity was assessed by dihydronicotinamide-adenine dinucleotide phosphate (NADPH) reduction followed by tetrahydrofolate (THF) formation. Enzyme assays were performed in 384-well, black, non-binding plates (Corning). Assay mixture consisted of reaction buffer (50 mM PIPES, pH 7.3, 0.02% Tween-20), NADPH (400 µM), BSA (1.5 mg/mL) and DTT (6 mM). The reaction was started by the addition of the enzyme substrate 7,8-dihydrofolate (diHF) (300 µM, final concentration). Final volume for the reaction mixture was 30 µL. NADPH fluorescence intensity (FI) was followed (excitation 340 nm/emission 445 nm) for 30 minutes at 25 °C using a ClarioSTAR® (BMG Labtech) plate reader. The acquired data was analysed using the MARS software (BMG Labtech). Enzyme titration experiments were performed by serial dilution of either wild-type or C89S *M. ulcerans* DHFR in assay reaction buffer. Experiments to determine MulDHFR and MulDHFR-C89S kinetic parameters (K_M, K_{cat}) were performed by serial dilution of diHF at fixed enzyme concentrations (10.0 nM). Half-maximal inhibitory concentrations (IC_{50}) were assessed by performing enzyme activity assays in the presence of increasing inhibitor concentrations, serially diluted in dimethyl sulfoxide (DMSO, Sigma-Aldrich). Compounds in 100% DMSO were transferred to the reaction plate using an automated liquid handler robot (Felix, Analytik Jena AG), and incubated for 30 min, at 25 °C, before the reaction was started by the addition of diHF. The final DMSO concentration in the assay mixture was 0.3 or 0.07 %, depending on the pin tool used to transfer the compounds to the assay plate. K_i values were calculated assuming competitive inhibition and used the Cheng-Prusoff relationship[36]: $K_i = IC_{50}/(1+ ([diHF]/K_{M,diHF}))$, where [diHF] is the diHF concentration used in the IC_{50} assay (300 µM). Graphical plots, enzyme kinetics, inhibitory pattern estimation and statistical analysis were performed in Prism-Graphpad 8.0. Values shown in graphical plots are the average of three data points $\pm$ standard deviations collected during a single experiment. All experiments were performed at least three times.

Protein crystallization and structure determination. For crystallization, NADPH and P218 were added to purified MulDHFR-C89S (12.5 mg.ml−1) at 6-fold molar excess. Sitting drops were set at 1:1 ratio composed of 400 nL of the protein-P218-NADPH

mixture to 400 nL reservoir solution. Crystallization experiments were performed at 14 °C. The best-diffracting crystals grew from the Morpheus crystallization screen (Molecular Dimensions) in a solution containing 12.5% (w/v) PEG 1000, 12.5% (w/v) PEG 3350, 12.5% (v/v) MPD, 0.03 M diethyleneglycol, 0.03 M triethyleneglycol, 0.03 M tetraethylene glycol, 0.03 M pentaethylene glycol and 0.1 M MOPS/HEPES-Na pH 7.5. Because of the makeup of the mother liquor, crystals were vitrified in liquid nitrogen with no additional cryo-protection. Diffraction data were collected at LS-CAT at the Advanced Photon Source Life Sciences Collaborative Access Team (APS LS-CAT) beamline 21-ID-D equipped with a Dectris Eiger 9M detector at a wavelength of 0.8666 Å. Data sets were reduced with the XDS package [37]. Molecular replacement (MR) was performed with Molrep[38] from the CCP4 package[39], using the *M. tuberculosis* structure as template (PDB ID 1DF7)[40]. Manual model building was performed using Coot[41], the structure was refined in reciprocal space with Phenix[42]. NADPH and P218 atoms were refined with full (1.0) occupancy. Structure validation was performed using MolProbity[43]. Structure factors and coordinates have been deposited in the PDB with the PDB ID 6UWW.

Results & Discussion

Recombinant Protein Production. To the best of our knowledge, recombinant production of *M. ulcerans* DHFR has not been reported before. We successfully produced recombinant wild-type MulDHFR in *E. coli* cells with an N-terminal poly-histidine tag to facilitate protein purification. The protein was purified from the clarified cell lysate using a combination of immobilized metal ion affinity chromatography (IMAC) and size exclusion chromatography. The N-terminal poly-histidine tag was not removed. Using LC-MS, we verified that the purified protein had the expected molecular weight (19,082.7 Da). This recombinant protein was used in biochemical assays and protein crystallization attempts.

Unfortunately, initial attempts to obtain crystals using recombinant wild-type MulDHFR were not successful (see below). To maximize chances of obtaining crystals we created a small series of mutant proteins with single or double residue changes hypothesized to alter crystallization properties[44]. We targeted non-conserved cysteine

or charged residues predicted to be surface exposed based on comparisons to the *M. avium* (Mav-DHFR) or *M. tuberculosis* structures[40] (overall sequence identity levels of 69 and 74% to MulDHFR, respectively). We then produced a mutant version of the enzyme in which MulDHFR cysteine 89 was replaced with a serine (MulDHFR-C89S). A sequence comparison to *M. avium* identified MulDHFR-E96 as a non-conserved and surface exposed residue. We mutated this residue to alanine in order to match the sequence of the *M. avium* DHFR, which was previously solved at high resolution. We also constructed the double mutant MulDHFR-C89S/E96A. Production of mutant proteins followed the same protocol used for the wild-type enzyme and the identity of the purified protein was verified by LC-MS.

Biochemical characterization of recombinant MulDHFR. To determine that both recombinant proteins were enzymatically active, we followed the DHFR reaction by monitoring the oxidation of NADPH into NADP catalysed by MulDHFR in the presence of 7,8-dihydrofolate (diHF). Using increasing amounts of the purified enzyme, we observed a dose-dependent reduction in NADPH fluorescence, indicating the recombinant MulDHFR was active. These enzyme titration curves were performed with an excess amount of cofactor NADPH (400 µM), and showed a linear relationship between the observed DHFR reaction rate and the final enzyme concentration used in the assay (ranging from 0.4 to 24 nM). Based on these results, we chose to use 10 nM of MulDHFR in all subsequent biochemical experiments. Further, our data showed that both wild-type and C89S MulDHFR have similar enzymatic activities (Fig 1A).

Determining the enzyme kinetic parameters for MulDHFR can help future drug discovery campaigns. Establishing the enzyme V_{max} and K_M for its substrate diHF ($K_{M,diHF}$) allows inhibitor constants (K_i) for diHF-competing ligands to be directly estimated from half-maximal inhibitory concentrations values (IC_{50}). K*i* values can then be used to compare the potency of the same compound for different enzymes. Further, determining how ligands impact an enzyme K_M and V_{max} can help establish their enzyme inhibition mechanisms. The kinetic parameters for the *M. tuberculosis* DHFR enzyme have already been established and were found to be comparable to those obtained for the enzymes from pathogenic Gram-positive and Gram-negative organisms, such as EcoDHFR and SauDHFR[23,45,46] (Table 1). To determine the enzyme kinetic parameters for wild-type MulDHFR, we first obtained initial velocity rates (v_0)

from reaction progress curves at increasing concentrations of the enzyme substrate diHF. Fitting these data to Michaelis-Menten kinetics allowed us to estimate a K_M value for the substrate diHF ($K_{M,diHF}$) of 12.3 + 4.9 µM, and a V_{max} value for the reaction of 123.7 nM.s^{-1}.ng (Fig 1B). Based on these values, we calculated a K_{cat} value of 6.2 s^{-1} for wild-type MulDHFR. Similar values were obtained for MulDHFR-C89S, further suggesting that the C89S point mutation did not interfere with the protein's enzymatic activity (Table 1). Our data indicated that the kinetic parameters of MulDHFR are comparable to those previously established for the enzyme from *M. tuberculosis*, *E. coli* and *S. aureus* (Table 1).

Enzyme inhibition studies identify P218 as a potent MulDHFR inhibitor. While DHFR inhibitors, such as TMP (Fig 1C, bottom), have found wide-use against Gram-positive and Gram-negative bacteria in the clinic[47], a similar therapeutic strategy for Mycobacterial infections has not been fully explored. Efforts to develop new antibiotics against mycobacterial infections has led to the exploration of anti-folate compounds targeting DHFR as treatment options. TMP bactericide activity is potentiated by sulfonamide-based antibiotics that target dihydropteroate synthase (DHPS), an enzyme upstream of DHFR in the folate pathway[48]. Sulfonamides can reduce DHFR substrate diHF, removing it from competing with TMP for the DHFR folate-binding site[47]. TMP is a potent inhibitor of EcoDHFR (K_i ~0.2 nM)[23] and SauDHFR (K_i ~4.4 nM)[46] but is only weakly active against MtbDHFR (K_i ~1.5 µM)[45]. To ascertain if TMP could inhibit MulDHFR, we obtained initial velocity (v_0) values for reactions performed at increasing concentrations of TMP. From this data we estimated the half-maximal inhibitory concentration of TMP for MulDHFR ($IC_{50,TMP}$ > 8,000 nM) and MulDHFR-C89S ($IC_{50,TMP}$ > 5,000 nM) (Fig 1D, and Fig S1), indicating that TMP is a weak inhibitor of MulDHFR and helping rationalize the reported lack of activity of this compound towards *M. ulcerans*[13].

P218 is a derivative of WR99210, a diaminopyridine compound originally developed for the *Plasmodium* enzyme and shown active against Mycobacteria[49,50] (Fig 1C, top). IC_{50} values of P218 for MulDHFR were obtained as described above for TMP and our data confirmed that P218 is a potent inhibitor of MulDHFR ($IC_{50,TMP}$ = 55.5 nM). Using the formalism of Cheng-Prussof [36], and the obtained $IC_{50,P218}$ and $K_{M,diHF}$ values, we computed an equilibrium inhibition constant ($K_{i,P218}$) of ~3.2 nM for P218 against

MulDHFR activity. We performed similar experiments for MulDHFR-C89S and obtained similar IC_{50} values for the mutant enzyme ($IC_{50,TMP}$ = 32.8 nM), showing P218 has similar potency for both the wild-type and the mutant enzyme used for the structural studies described below.

The crystal structure of MulDHFR-C89S bound to cofactor NADPH and inhibitor P218. Currently, there are no MulDHFR structures available. To better understand P218 binding to MulDHFR, and to provide a starting point for future structure-based drug design programs for this enzyme, we obtained the co-crystal structure of MulDHFR-C89S bound to P218 and cofactor NADPH to a resolution of 0.9 Å (Fig. 2). As we could not obtain co-crystals of P218 bound to the wild-type protein, all structural work described below was performed with the MulDHFR-C89S mutant. In the light of our biochemical analysis above, we are confident the C89S mutation caused minimum, if any, disturbance to the native enzyme structure. MulDHFR-C89S crystals were obtained in the presence of excess cofactor NADPH and inhibitor P218. We used the structure of MtbDHFR (PDB ID 1DF7) as a search model in molecular replacement to solve the crystallographic phase problem (Table S1). No density was observed for the first two N-terminal residues in MulDHFR-C89S, likely due to disorder, and the final protein model consisted of residues 3-165 (Fig 2). Both the ligand P218 and the cofactor NADPH could be placed unambiguously into the electron density unfilled by the protein model (OMIT map shown for P218 in Fig. 2). MulDHFR-C89S crystal structure is similar to that of its counterpart from *M. tuberculosis* (root mean square deviation, r.m.s.d. = 0.45 Å for 135 equivalent Cα atoms), as expected from the high identity levels between these two proteins (74%) (Fig S2).

Our co-crystal structure offered a detailed view of the binding of P218 to MulDHFR-C89S (Fig. 3). The ligand 2,4-diaminopyrimidine (DAP) moiety anchored P218 deep into the enzyme active site, sandwiched between the aromatic side chain of Phe33 and cofactor NADPH amide group. Further, the amino groups in P218 DAP make hydrogen bonds to side chain atoms from residues Asp29 and Tyr106, and to main chain atoms from residues Ile7 and Ile100 in MulDHFR-C89S. P218 five-atom linker confers the ligand enough flexibility for its benzyl group to point away from Phe41 side chain while allowing the ligand α-carboxylate group to interact via a bidentate hydrogen bond to Arg62. Structurally equivalent arginine residues to MulDHFR Arg62 are conserved

amongst DHFR enzymes from different organisms, as this residue interacts directly with the substrate dihydrofolate α-carboxylate group[25,51].

The sequence and structural conservation between human and *M. ulcerans* DHFR enzymes may raise concerns about the safety of using anti-folates as a therapeutic strategy to treat Buruli Ulcer. However, P218 is ~1000-fold more active against MulDHFR, as compared to the human enzyme (HsaDHFR $K_{i,P218}$ ~2.8 μM)[52]. The co-structure of P218 bound to HsaDHFR revealed that the ligand α-carboxylate group pointed away from the enzyme dihydrofolate-interacting arginine residue (Arg70 in HsaDHFR). In the human enzyme, residues Phe31 (Leu30 in MulDHFR) and Gln35 (Lys34 in MulDHFR) sterically interfere with P218 binding, and prevent the compound α-carboxylate group from reaching the conserved arginine residue (Fig. 3). The resulting difference in ligand binding mode is thought to be responsible for P218 low activity towards the human enzyme.

Conclusion

P218 is a safe DHFR inhibitor already under clinical investigation for malaria[52] and here we have identified it as a potent inhibitor of the *M. ulcerans* DHFR enzyme. Our structural and biochemical characterization of *M. ulcerans* DHFR and its interaction with P218 offers an opportunity to further develop P218 as a therapeutic strategy against Buruli ulcer. To reduce the chances of emerging resistance to anti-folates, we suggest P218 be used in combination with other antimicrobial agents currently used for Buruli ulcer treatment, especially those that can be administered orally and do not have severe side effects, such as rifampin[7–9].

307

Table 1 - Enzyme kinetics and inhibition parameters of TMP and P218 for DHFR from various bacteria.

DHFR	$K_{M,diHF}$ (μM)	IC_{50} (nM)		Ki (nM)		references
		TMP	P218	TMP	P218	
MulDHFR	18.6 (12.8-31.2) *	> 8,000	55.5 (41.9-73.0) *	ND	3.2	This work
MtbDHFR	4.5±0.6	16.5±2.5	ND	1,500	ND	[45]
EcoDHFR	0.8±0.3	0.020±0.002	ND	0.17±0.06	ND	[23]
SauDHFR	43.7 ± 5.9	0.014	ND	4.4	ND	[46]

308 * 95% confidence interval

309

FIGURE 1

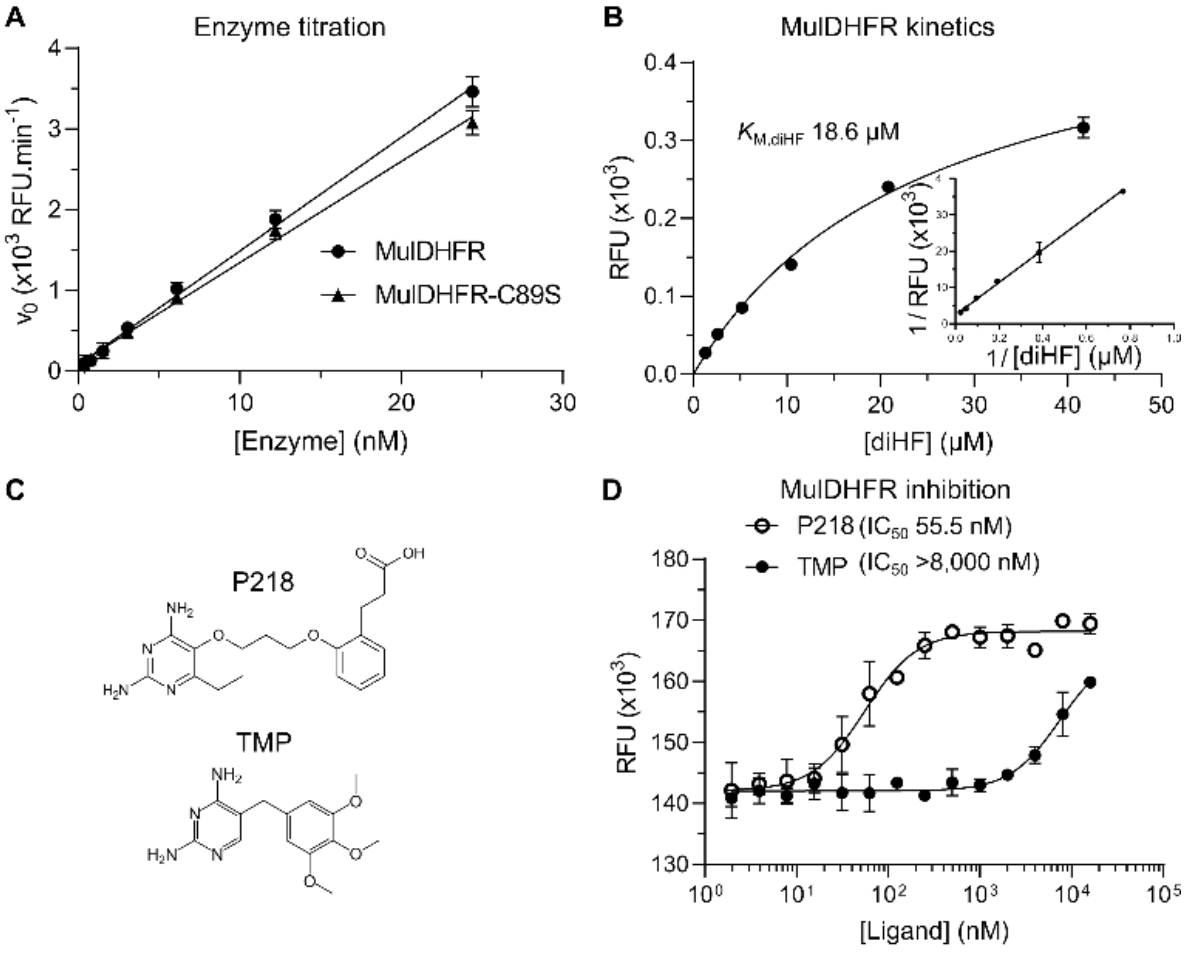

Fig. 1 - MulDHFR and MulDHFR-C89S have similar enzymatic properties and can be inhibited by P218. (A) Linear relationship between increasing concentrations of wild-type (circles) or C89S mutant (triangles) MulDHFR and the reaction rates (initial velocities - v_0). **(B)** Hyperbolic relationship between substrate concentration and the rate (initial velocity - normalized v_0) of the DHFR-catalysed reaction for the wild-type enzyme. The inset shows the Lineweaver-Burk plot of the same kinetic data. The value of the Michaelis-Menten constant (K_M -defined as the concentration of substrate diHF needed to reach the reaction's half-maximal velocity) was obtained from the x-axis intercept in Lineweaver-Burk plot. (**C**) Chemical structures of P218 (top) and trimethoprim (TMP, bottom. (**D**) Enzyme inhibition of wild-type MulDHFR by TMP (filled symbols) and P218 (empty symbols). The half-maximal inhibitory concentration (IC_{50}) for each compound is shown in parenthesis. Data shown are mean ± SD of triplicates.

Figure 2

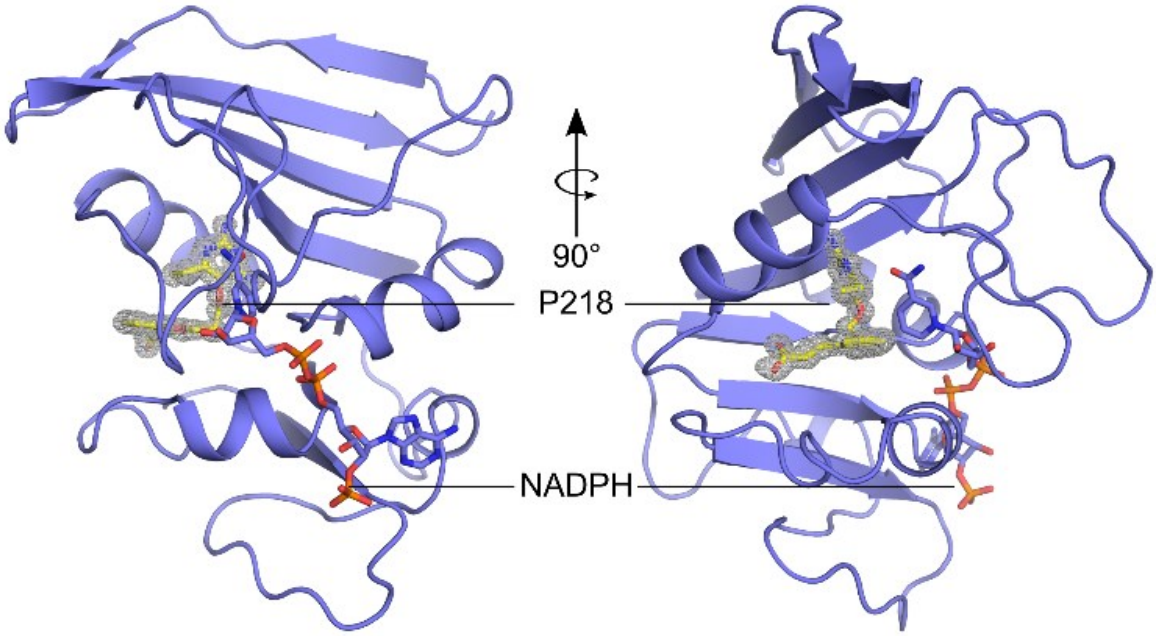

Fig. 2 - The structure of MulDHFR-C89S bound to P218 and NADPH. (A-B) Cartoon representation of the MulDHFR-C89S structure. P218 and NADPH molecules are shown as stick. P218 is covered by a polder OMIT map [53] (grey mesh represents the mFobs-DFmodel OMIT difference density contoured at 3.0 σ).

Figure 3

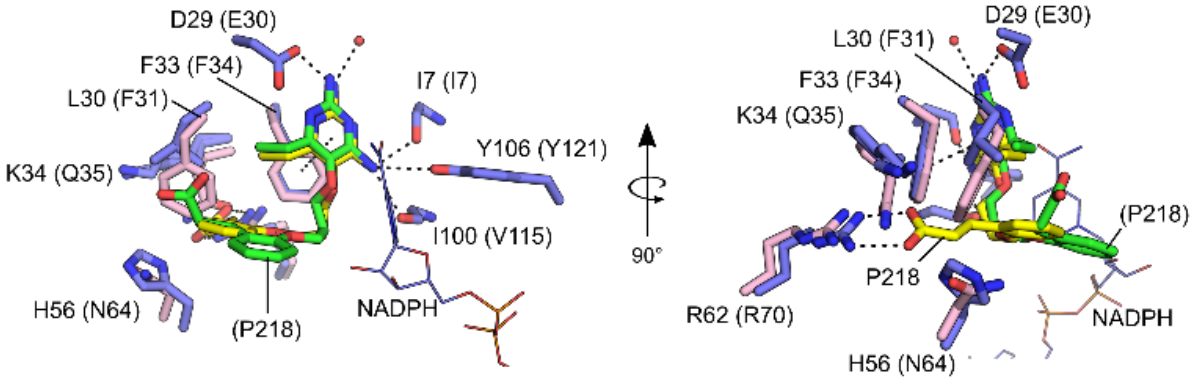

Fig. 3 - Details of P218 binding to MulDHFR and HsaDHFR. Amino acid residues within the folate-binding site of MulDHFR-C89S (blue sticks) and HsaDHFR (pink sticks). Residues / ligands in parenthesis are for the human enzyme. The ligand P218 is shown as sticks in yellow, for the MulDHFR co-structure, or green, for the HsaDHFR co-structure. The cofactor NADPH as seen in the MulDHFR co-structure is also shown (lines). Dashed lines indicate possible hydrogen bonds between the ligand and atoms from the protein or the solvent (shown as a red sphere) in MulDHFR-C89S crystals.

Conflicts of interest

There are no conflicts to declare.

Acknowledgements

This work was supported by the Brazilian agencies FAPESP (Fundação de Amparo à Pesquisa do Estado de São Paulo) (2013/50724-5 and 2014/50897-0) and CNPq (Conselho Nacional de Desenvolvimento Científico e Tecnológico) (465651/2014-3). The SGC is a registered charity (number 1097737) that receives funds from AbbVie, Bayer Pharma AG, Boehringer Ingelheim, Canada Foundation for Innovation, Eshelman Institute for Innovation, Genome Canada, Innovative Medicines Initiative (EU/EFPIA) [ULTRA-DD grant no. 115766], Janssen, Merck KGaA Darmstadt Germany, MSD, Novartis Pharma AG, Ontario Ministry of Economic Development and Innovation, Pfizer, Takeda, and Wellcome [106169/ZZ14/Z]. This project has been funded in part with Federal funds from the National Institute of Allergy and Infectious Diseases, National Institutes of Health, Department of Health and Human Services, under Contract No. HHSN272201700059C. We thank the staff of the Life Sciences Core Facility (LaCTAD) at UNICAMP for the Genomics and Proteomics analysis.

Notes and references

1 F. S. Sarfo, R. Phillips, M. Wansbrough-Jones and R. E. Simmonds, *Cell. Microbiol.*, 2016, **18**, 17

2 K. M. George, D. Chatterjee, G. Gunawardana, D. Welty, J. Hayman, R. Lee and P. L. C. Small, *Science*, **5403**, 854

3 3 D. S. Walsh, F. Portaels and W. M. Meyers, *Trans. R. Soc. Trop. Med. Hyg.*, 2008, **102**, 969.

4 WHO Meeting on Buruli ulcer and other skin NTDs - Final Report, 2019.

5 T. Wagner, M. E. Benbow, T. O. Brenden, J. Qi and R. C. Johnson, *Int. J. Health Geogr.*, 2008, **7**, 25.

6 M. Debacker, F. Portaels, J. Aguiar, C. Steunou, C. Zinsou, W. Meyers and M. Dramaix, *Emerg. Infect. Dis.*, 2006, **12**, 1325.

7 S. Klis, Y. Stienstra, R. O. Phillips, K. M. Abass, W. Tuah and T. S. van der Werf, *PLoS Negl. Trop. Dis.*,2014, **8**, e2739.

8 P. J. Converse, D. V. Almeida, R. Tasneen, V. Saini, S. Tyagi, N. C. Ammerman, S. Y. Li, N. M. Anders, M. A. Rudek, J. H. Grosset and E. L. Nuermberger, *PLoS Negl. Trop. Dis.*, 2018, **12**, e0006728.

9 N. Scherr, R. Bieri, S. S. Thomas, A. Chauffour, N. P. Kalia, P. Schneide, M. T. Ruf, A. Lamelas, M. S. S. Manimekalai, G. Grüber, N. Ishii, K. Suzuki, M. Tanner, G. C. Moraski, M. J. Miller, M. Witschel, V. Jarlier, G. Pluschke and K. Pethe, *Nat. Commun.*, 2018, **9**, 5370.

10 Y. Minato, J. M. Thiede, S. L. Kordus, E. J. McKlveen, B. J. Turman and A. D. Baughn, *Antimicrob. Agents Chemother.*, 2015, **59**, 5097.

11 M. R. Nixon, K. W. Saionz, M. S. Koo, M. J. Szymonifka, H. Jung, J. P. Roberts, M. Nandakumar, A. Kumar, R. Liao, T. Rustad, J. C. Sacchettini, K. Y. Rhee, J. S. Freundlich and D. R. Sherman, *Chem. Biol.*, 2014, **21**, 819.

12 S. R. Pattyn and J. van Ermengem, *Int. J. Lepr. Other Mycobact. Dis.*, 1968, **36**, 427.

13 A. M. Dhople, *J. Antimicrob. Chemother.*, 2001, **47**, 93.

14 A. M. Dhople, *Int. J. Antimicrob. Agents*, 2002, **19**, 71.

15 A. M. Dhople, *Int. J. Antimicrob. Agents*, 1999, **12**, 319.

16 A. M. Dhople, *Arzneimittel-Forschung/Drug Res*., 1999, **49**, 267.

17 A. M. Dhople, I. Ortega, J. K. Seydel and G. D. Gardner, *Indian J. Lepr.*, 1990, **62**, 76.

18 A. Kumar, A. Guardia, G. Colmenarejo, E. Pérez, R. R. Gonzalez, P. Torres, D. Calvo, R. M. Gómez, F. Ortega, E. Jiménez, R. C. Gabarro, J. Rullás, L. Ballell and D. R. Sherman, *ACS Infect. Dis.*, 2016, **1**, 604.

19 B. Hajian, E. Scocchera, S. Keshipeddy, N. G-Dayanandan, C. Shoen, J. Krucinska, S. Reeve, M. Cynamon, A. C. Anderson and D. L. Wright, *PLoS One*, 2016, **11**, e0161740.

20 B. Hajian, E. Scocchera, C. Shoen, J. Krucinska, K. Viswanathan, N. G-Dayanandan, H. Erlandsen, A. Estrada, K. Mikušová, J. Korduláková, M. Cynamon and D. Wright, *Cell Chem. Biol.*, 2019, **26**, 781.

21 J. Zheng, E. J. Rubin, P. Bifani, V. Mathys, V. Lim, M. Au, J. Jang, J. Nam, T. Dick, J. R. Walker, K. Pethe and L. R. Camacho, *J. Biol. Chem*., 2013, **388**, 23447.

22 T. P. Stinear, T. Seemann, S. Pidot, W. Frigui, G. Reysset, T. Garnier, G. Meurice, D. Simon, C. Bouchier, L. Ma, M. Tichit, J. L. Porter, J. Ryan, P. D. R. Johnson, J. K. Davies, G. A. Jenkin, P. L. C. Small, L. M. Jones, F. Tekaia, F. Laval, M. Daffé, J. Parkhill and S. T. Cole, *Genome Res.*, 2007, **17**, 192.

23 M. Cammarata, R. Thyer, M. Lombardo, A. Anderson, D. Wright, A. Ellington and J. S. Brodbelt, *Chem. Sci.*, 2017, **8**, 4062.

24 H. H. Locher, H. Schlunegger, P. G. Hartman, P. Angehrn and R. L. Then, *Antimicrob. Agents Chemother.*, **40**, 1376.

25 M. R. Sawaya and J. Kraut, *Biochemistry*, 1997, **36**, 586.

26 R. De Groot, M. Sluijter, A. D. De Bruyn, J. Campos, W. H. F. Goessens, A. L. Smith and P. W. M. Hermans, *Antimicrob. Agents Chemother.*, 1996, **40**, 2131.

27 G. E. Dale, C. Broger, A. D'Arcy, P. G. Hartman, R. DeHoogt, S. Jolidon, I. Kompis, A. M. Labhardt, H. Langen, H. Locher, M. G. P. Page, D. Stüber, R. L. Then, B. Wipf and C. Oefner, *J. Mol. Biol.*, 1997, **266**, 23.

28 A. Pikis, J. A. Donkersloot, W. J. Rodriguez and J. M. Keith, *J. Infect. Dis.*, 1998, **178**, 700.

29 P. Myler, R. Stacy, L. Stewart, B. Staker, W. Van Voorhis, G. Varani and G. Buchko, *Infect. Disord. - Drug Targets*, 2009, **9**, 493.

30 R. Stacy, D. W. Begley, I. Phan, B. L. Staker, W. C. Van Voorhis, G. Varani, G. W. Buchko, L. J. Stewart and P. J. Myler, *Acta Crystallogr. Sect. F Struct. Biol. Cryst. Commun.*, 2011, **67**, 979.

31 R. Choi, A. Kelley, D. Leibly, S. Nakazawa Hewitt, A. Napuli and W. Van Voorhis, *Acta Crystallogr. Sect. F Struct. Biol. Cryst. Commun.*, 2011, **67**, 998.

32 D. A. Serbzhinskiy, M. C. Clifton, B. Sankaran, B. L. Staker, T. E. Edwards and P. J. Myler, *Acta Crystallogr. Sect. F Struct. Biol. Commun.*, 2015, **71**, 594.

33 C. M. Bryan, J. Bhandari, A. J. Napuli, D. J. Leibly, R. Choi, A. Kelley, W. C. Van Voorhis, T. E. Edwards and L. J. Stewart, *Acta Crystallogr. Sect. F Struct. Biol. Cryst. Commun.*, 2011, **67**, 1010.

34 F. W. Studier, *Protein Expr. Purif.*, 2005, **41**, 207.

35 M. Vedadi, J. Lew, J. Artz, M. Amani, Y. Zhao, A. Dong, G. A. Wasney, M. Gao, T. Hills, S. Brokx, W. Qiu, S. Sharma, A. Diassiti, Z. Alam, M. Melone, A. Mulichak, A. Wernimont, J. Bray, P. Loppnau, O. Plotnikova, K. Newberry, E. Sundararajan, S. Houston, J. Walker, W. Tempel, A. Bochkarev, I. Kozieradzki, A. Edwards, C. Arrowsmith, D. Roos, K. Kain and R. Hui, *Mol. Biochem. Parasitol.*, 2007, **151**, 100.

36 C. Yung-Chi and W. H. Prusoff, *Biochem. Pharmacol.*, 1973, **22**, 3099.

37 W. Kabsch, *Acta Crystallogr. Sect. D Biol. Crystallogr.*, 2010, **66**, 125.

38 A. Vagin and A. Teplyakov, *J. Appl. Crystallogr.*, 1997, **30**, 1022.

39 M. D. Winn, C. C. Ballard, K. D. Cowtan, E. J. Dodson, P. Emsley, P. R. Evans, R. M. Keegan, E. B. Krissinel, A. G. W. Leslie, A. McCoy, S. J. McNicholas, G. N. Murshudov,

N. S. Pannu, E. A. Potterton, H. R. Powell, R. J. Read, A. Vagin and K. S. Wilson, *Acta Crystallogr. Sect. D Biol. Crystallogr.*, 2011, **67**, 235.
40 R. Li, R. Sirawaraporn, P. Chitnumsub, W. Sirawaraporn, J. Wooden, F. Athappilly, S. Turley and W. G. J. Hol, *J. Mol. Biol.*, 2000, **295**, 307.
41 P. Emsley, B. Lohkamp, W. G. Scott and K. Cowtan, *Acta Crystallogr. Sect. D Biol. Crystallogr.*, 2010, **66**, 486.
42 P. D. Adams, P. V. Afonine, G. Bunkóczi, V. B. Chen, I. W. Davis, N. Echols, J. J. Headd, L. W. Hung, G. J. Kapral, R. W. Grosse-Kunstleve, A. J. McCoy, N. W. Moriarty, R. Oeffner, R. J. Read, D. C. Richardson, J. S. Richardson, T. C. Terwilliger and P. H. Zwart, *Acta Crystallogr. Sect. D Biol. Crystallogr.*, 2010, **66**, 213.
43 V. B. Chen, W. B. Arendall, J. J. Headd, D. A. Keedy, R. M. Immormino, G. J. Kapral, L. W. Murray, J. S. Richardson and D. C. Richardson, *Acta Crystallogr. Sect. D Biol. Crystallogr.*, 2010, **66**, 12.
44 Z. S. Derewenda, *Structure*, 2004, **12**, 529.
45 E. L. White, L. J. Ross, A. Cunningham and V. Escuyer, *FEMS Microbiol. Lett.*, 2004, **232**, 101.
46 C. R. Bourne, E. W. Barrow, R. A. Bunce, P. C. Bourne, K. D. Berlin and W. W. Barrow, *Antimicrob. Agents Chemother.*, 2010, **54**, 3825.
47 A. Wróbel, K. Arciszewska, D. Maliszewski and D. Drozdowska, *J. Antibiot. (Tokyo)*, 2020, **73**, 5.
48 O. Sköld, *Veterinary Research*, 2001, **32**, 261.
49 S. C. C. Meyer, S. K. Majumder and M. H. Cynamon, *Antimicrob. Agents Chemother.*, 1995, **39**, 1862.
50 A. Kumar, M. Zhang, L. Zhu, R. P. Liao, C. Mutai, S. Hafsat, D. R. Sherman and M. W. Wang, *PLoS One*, 2012, **7**, e39961.
51 J. A. Ribeiro, S. M. Chavez-Pacheco, G. S. De Oliveira, C. Dos Santos Silva, J. H. P. Giudice, G. A. Libreros-Zúñiga and M. V. B. Dias, *Acta Crystallogr. Sect. D Struct. Biol.*, 2019, **75**, 682.
52 Y. Yuthavong, B. Tarnchompoo, T. Vilaivan, P. Chitnumsub, S. Kamchonwongpaisan, S. A. Charman, D. N. McLennan, K. L. White, L. Vivas, E. Bongard, C. Thongphanchang, S. Taweechai, J. Vanichtanankul, R. Rattanajak, U. Arwon, P. Fantauzzi, J. Yuvaniyama, W. N. Charman and D. Matthews, *Proc. Natl. Acad. Sci.*, 2012, **109**, 16823.
53 D. Liebschner, P. V. Afonine, N. W. Moriarty, B. K. Poon, O. V. Sobolev, T. C. Terwilliger and P. D. Adams, *Acta Crystallogr. Sect. D Struct. Biol.*, 2017, **73**, 148.

Supplementary Material

Identification of P218 as a potent inhibitor of *M. ulcerans* DHFR

Gustavo Pelicioli Riboldi,[ab] Rachael Zigweid,[c] Peter J. Myler,[cd] Stephen J. Mayclin,[cd] Rafael Miguez Couñago,[ab*] Bart L. Staker[*c]

a. Centro de Química Medicinal (CQMED), Centro de Biologia Molecular e Engenharia Genética (CBMEG), Universidade Estadual de Campinas (UNICAMP), Campinas, SP, 13083-875, Brazil.

b. Structural Genomics Consortium, Departamento de Genética e Evolução, Instituto de Biologia, UNICAMP, Campinas, SP, 13083-886, Brazil.

c. Center for Infectious Disease Research, Seattle Children's Research Institute, Seattle, Washington, 98109, USA.

d. Department of Pediatrics, University of Washington, Seattle, Washington, 91895, USA.

* rafael.counago@unicamp.br; bart.staker@seattlechildrens.org

Supplementary Table S1. Crystallographic data and refinement statistics for MulDHFR-C89S crystals.

Data collection	
Crystal	Native
PDB ID	6UWW
X-ray source	APS LS-CAT 21-ID-D
Wavelength (Å)	0.8666
Space group	P 1 2_1 1
Cell dimensions	
a, *b*, *c* (Å)	28.73, 66.20, 44.52
α, β, γ (°)	90.000, 91.614, 90.000
Resolution (Å)	50-0.92 (0.94-0.92)
No. of unique reflections*	112,854 (8,042)
R_{merge} (%)	3.6 (49.1)
Mean I/σI	14.66 (2.01)
Mean $CC_{1/2}$	99.9 (74.8)
Completeness (%)	98.1 (94.7)
Redundancy	3.5 (2.9)
Refinement Statistics	
Resolution (Å)	50-0.92 (0.94-0.92)
R_{work} / R_{free} (%)	13.15 (21.59) / 14.54 (22.67)
No. of atoms / Mean B-factor (Å)	
Protein atoms	1,331 / 12.2
Solvent atoms	271/ 29.8
NADPH/P218 atoms	84 / 13.9
RMSD bond lengths	0.009 Å
RMSD bong angles	1.29°
Ramachandran plot (%)	
Favored	98.8
Allowed	1.2
Outliers	0

Data for the outmost shell are given in parentheses.

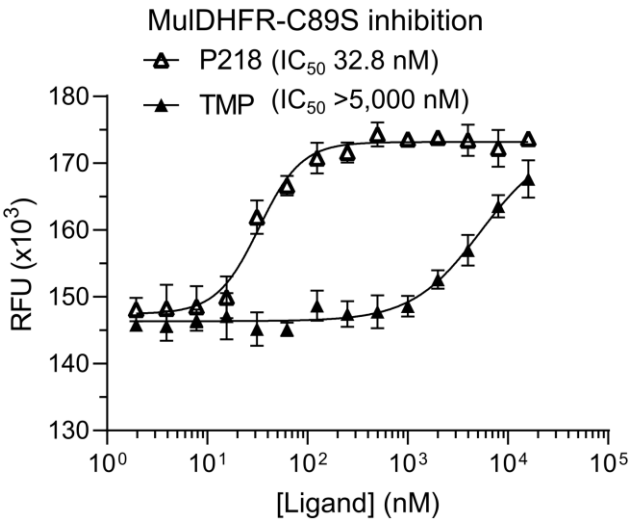

Supplementary Figure S1 - Enzyme inhibition of mutant MulDHFR-C89S by TMP (filled symbols) and P218 (empty symbols). The half-maximal inhibitory concentration (IC_{50}) for each compound is shown in parenthesis. Data shown are mean ± SD of triplicates.

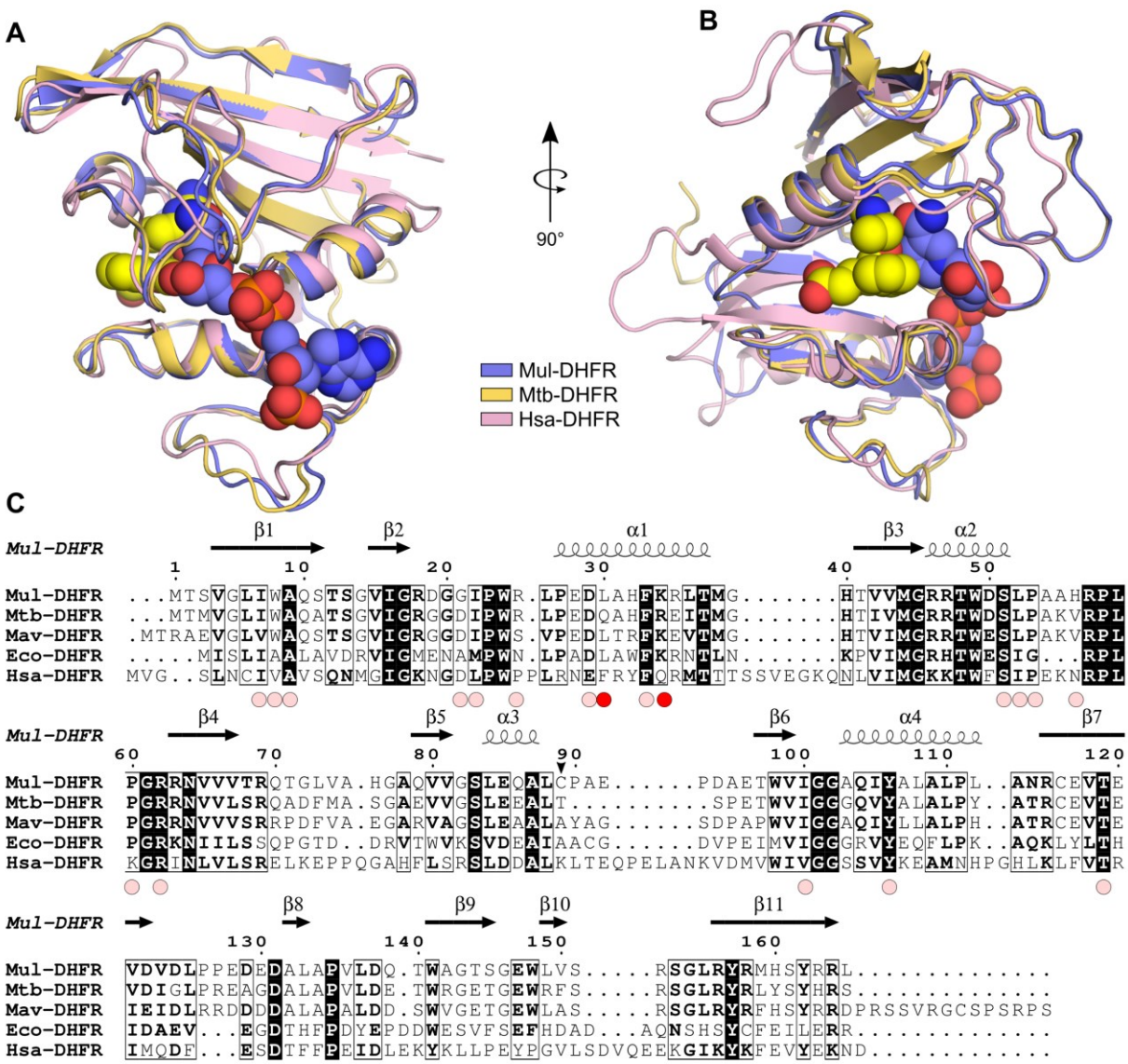

Supplementary Fig. S2 - The structure of MulDHFR-C89S bound to P218 and NADPH reveals a conserved DHFR architecture. (**A-B**) Superposition of MulDHFR-C89S (blue cartoon) onto the P218-NADPH-bound structures of *M. tuberculosis* (yellow cartoon, PDB ID5U26) and human (pink cartoon, PDB ID 4DDR)[1] enzymes. P218 and NADPH, as seen in the MULDHFR-C89S co-structure, are shown as van der Waal spheres. **(C)** Structure-based sequence alignment of *M. ulcerans* (Mul-), *M. tuberculosis* (Mtb-), *M. avium* (Mav-), *E. coli* (Eco-), and human (Hsa-) DHFR. Pink circles indicate structurally-equivalent residues within a 4 Å radius of ligand P218, as seen in our MulDHFR-C89S structure. Red circles indicate structurally-equivalent residues thought responsible for sterically preventing P218 binding to the human enzyme. The black arrowhead indicates the position of Cys89 in MulDHFR mutated to a serine to improve protein crystallization. Absolutely conserved residues are indicated by a black background. Similar residues are shown in bold and framed in a box. The secondary structure

(α-helices, shown as coils; and β-sheets, shown as arrows), and the numbering shown in the top line are for MulDHFR. Protein sequence / structures used in were: Mul-DHFR (UniProt ID A0PQG8, PDB ID 6UWW) (this work), Mtb-DHFR (UniProt ID P9WNX1, PDB ID 5U26), Mav-DHFR (UniProt ID O30463, PDB ID 2W3W), Eco-DHFR (UniProt ID P0ABQ4, PDB ID 1RF7)[2], and Hsa-DHFR (UniProt ID P00374, PDB ID 4DDR)[1]. Structural alignment by PROMALS3D [3].

Supplementary References:

1 Y. Yuthavong, B. Tarnchompoo, T. Vilaivan, P. Chitnumsub, S. Kamchonwongpaisan, S. A. Charman, D. N. McLennan, K. L. White, L. Vivas, E. Bongard, C. Thongphanchang, S. Taweechai, J. Vanichtanankul, R. Rattanajak, U. Arwon, P. Fantauzzi, J. Yuvaniyama, W. N. Charman and D. Matthews, *Proc. Natl. Acad. Sci.*, 2012, **109**, 16823–16828.

2 M. R. Sawaya and J. Kraut, *Biochemistry*, 1997, **36**, 586–603.

3 J. Pei and N. V. Grishin, *Bioinformatics*, 2007, **23**, 802–808.